from this type of reaction was present in the other product mixtures it was not detected. It is possible that it is present in other product mixtures, however, since no effort was made to prove its absence.

Malononitrile was treated with tetrafluoroethylene and benzoyl peroxide but the products were coupled radicals with essentially no incorporation of tetrafluoroethylene.

Experimental Section

The procedure used has been described before.[1-4] The results of the experiments are presented in Table III.

Acknowledgment. Thanks are given to C. B. Strow, Jr., for running the NMR spectra.

Registry No. H-CH_2CN, 75-05-8; H-$CHClCN$, 107-14-2; H-CCl_2CN, 3018-12-0; Cl-CCl_2CN, 545-06-2; $CNCH_2CH_2CN$, 110-61-2; $CNCHClCH_2CN$, 84332-52-5; $CNCHClCHClCN$, 84304-00-7; $CNCHClCCl_2CN$, 84304-01-8; $CNCCl_2CCl_2CN$, 6613-50-9; tetrafluoroethylene, 116-14-3; acetic acid, 64-19-7; ethyl acetate, 141-78-6.

References and Notes

(1) Moore, L. O. *J. Phys. Chem.* **1970**, *74*, 3603.
(2) Moore, L. O. *J. Phys. Chem.* **1971**, *75*, 2075.
(3) Moore, L. O. *Can. J. Chem.* **1971**, *49*, 666.
(4) Moore, L. O. *Macromolecules* **1983**, *16*, 357.
(5) Walling, C. "Free Radicals in Solution"; Wiley: New York, 1957; p 150.
(6) This distribution by using an averaging method to calculate chain-transfer constants gives the same result as if the single concentrations of each type of atom and probabilities of reaction are used.
(7) Hanford, W. E. U.S. Patent 2 411 158, Nov 19, 1946 (to E. I. du Pont de Nemours and Co.).
(8) Hanford, W. E.; Joyce, R. M., Jr. U.S. Patent 2 562 547, Jul 31, 1951 (to E. I. du Pont de Nemours and Co.).
(9) Cadogen, J. I. G.; Hey, D. H.; Sharp, J. T. *J. Chem. Soc. B* **1966**, 933.
(10) We ran one experiment reacting diethyl malonate with tetrafluoroethylene, but there was extensive coupling of malonate radicals and the NMR spectrum was difficult to interpret.
(11) Wineman, R. J.; Kliss, R. M.; Matthews, C. N. U.S. Patent 3 231 523, Jan 25, 1966 (to Monsanto Chemical Co.).
(12) In partly chlorinated methanes and ethanes, phenyl radicals abstract only hydrogen, while they abstract chlorine only from perchlorinated materials; for example, see: Hey, D. H.; Peters, J. *J. Chem. Soc.* **1960**, 79.
(13) Freidlina, R. Kh.; Terentev, A. B.; Ikonikov, N. S. *Dokl. Akad. Nauk SSSR* **1970**, *193*, 605.
(14) Dedek, V.; Fikar, J. *Collect. Czech. Chem. Commun.* **1969**, *34*, 3769.

Ordered Structure in Block Polymer Solutions. 2. Its Effect on Rheological Behavior†

Takeji Hashimoto,* Mitsuhiro Shibayama, and Hiromichi Kawai

Department of Polymer Chemistry, Faculty of Engineering, Kyoto University, Kyoto 606, Japan

Hiroshi Watanabe and Tadao Kotaka

Department of Polymer Science, Faculty of Science, Osaka University, Toyonaka, Osaka 560, Japan. *Received March 25, 1982*

ABSTRACT: Polystyrene–polybutadiene (SB) diblock polymer in *n*-tetradecane forms an ordered microdomain structure in which spherical microdomains composed of polystyrene (PS) block chains are dispersed in a solution of polybutadiene (PB) block chains in a simple-cubic-like lattice. The superlattice, which is stabilized by the conformational entropy of the PB chains, is shown to be a primary cause of nonlinear and plastic flow behavior of the solution with an apparent yield stress proportional to ϕ_P, the volume fraction of SB in the solution. The superlattice starts to be distorted, resulting in loss of long-range spatial order of the microdomain structures, at temperatures higher than T_d, the lattice disordering temperature. The lattice disordering is shown to cause an increase of the line profile of the small-angle X-ray scattering (SAXS) maximum and also a discontinuous change of the Bragg spacing with temperature. It is also shown that with increasing temperature across T_d, the flow behavior changes from nonlinear and plastic to linear and non-Newtonian behavior, and the apparent yield stress vanishes. Upon further increase of temperature above the critical temperature T_c, the microdomain structure is dissolved into, more or less, a homogeneous solution of PS and PB; i.e., the system undergoes an order-to-disorder transition. This transition causes the change of the flow behavior from non-Newtonian behavior. An effect of adding homopolybutadiene into the solution on the lattice-disordering phenomenon is also discussed.

I. Introduction

In the previous paper[1] of this series we have explored the microdomain structure of polystyrene–polybutadiene (SB) block polymer in a selective solvent of *n*-tetradecane, good for polybutadiene (PB) chains but very poor for polystyrene (PS) chains as a function of concentration and temperatures. In this paper we shall explore some effects of the microdomain structure and its superlattice on the rheological behavior of the solution.

In section III we shall present some results of small-angle X-ray scattering (SAXS), especially the results indicating two thermal transitions, (i) the lower temperature one associated with a thermal destruction of the *superlattice* (i.e., simple-cubic-like spatial arrangement of the spherical microdomains of PS dispersed in the matrix of PB solution) at the *lattice-disordering* temperature T_d (section III-1) and (ii) the higher the temperature one associated with an *order-to-disorder transition*[2] involving dissolution of the microdomain structure to a nearly homogeneous molecular mixture at the critical temperature T_c (section III-2). Some effects of the *lattice disordering* on the temperature dependence of the line profiles of SAXS maximum and that of the Bragg spacing shall be discussed in section III-1 and III-3, respectively.

In section IV we shall describe changes of the rheological behavior of the solutions with temperature, especially at

† Dedicated to Professor Dr. D. J. Meier on the occasion of his 60th birthday.

0024-9297/83/2216-0361$01.50/0

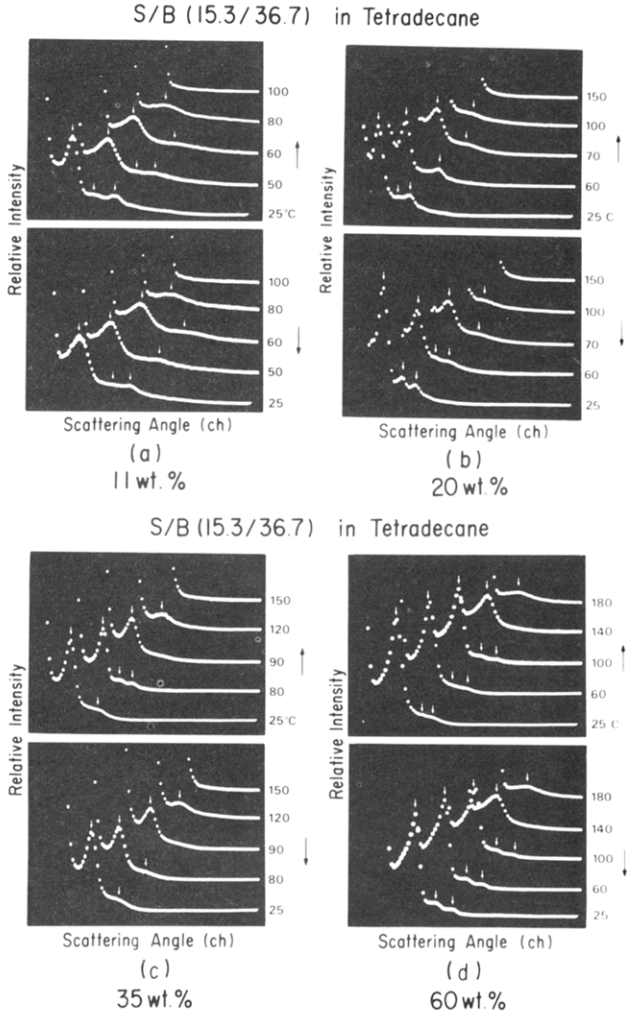

Figure 1. Oscilloscope displays on the variations of the SAXS profiles with heating (upper row) and cooling (bottom row) of *n*-tetradecane solutions of the SB block polymers at various concentrations: (a) 11, (b) 20, (c) 35, and (d) 60 wt%. The change of the profile with temperature is essentially reversible. The origin of each scattering profile is shifted diagonally. The white arrows indicate the scattering maxima arising from interparticle interference at relative angular positions of $1:\sqrt{2}:\sqrt{3}$. The first-order peak disappears at $T \geq T_c$, and the peaks at $\sqrt{2}$ and $\sqrt{3}$ may overlap into a single broad peak or dissappear at $T_d \leq T (<T_c)$.

the two transition temperatures T_d and T_c (section IV-1) and with concentration (section IV-2). At temperatures below T_d, it is shown that the solution exhibits an apparent *yield stress* that scales with ϕ_P where ϕ_P is the volume fraction of SB in the solution (section IV-2). Below the yield stress, the dynamic behavior of the solution is described by linear elasticity with the shear modulus also approximately proportional to ϕ_P. In section IV-3 we shall derive a master relationship between the structural parameter $\delta s/s_m$ and the rheological parameter G or σ_0. Finally in section V we shall discuss some effects of adding homopolybutadiene to the solution on the superlattice and on the rheological behavior.

II. Experimental Methods

Details of the sample preparation and SAXS measurements as well as the rheological measurements were described elsewhere by Kotaka et al.[3] and Hashimoto et al.[1] A commericial SB block polymer (Phillips Petroleum, Solprene 1205) was used as received without further purification. The polymer has number-average molecular weight 5.2×10^4 and styrene content 29.5 wt %. The *n*-tetradecane solutions (coded as C14) were prepared by mixing prescribed amounts of SB and solvent with an excess amount of methylene chloride, which was subsequently evaporated completely. *n*-Tetradecane has almost complete selectivity, a good solvent for PB and a poor solvent for PS chains.

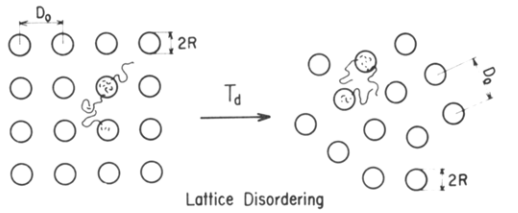

Figure 2. Schematic diagram showing the lattice disordering. At temperatures below the lattice-disordering temperature, T_d, the solution possesses a long-range spatial order of the spherical microdomains. At temperatures $T > T_d$, the solution possesses only a short-range liquid-like order of the microdomains.

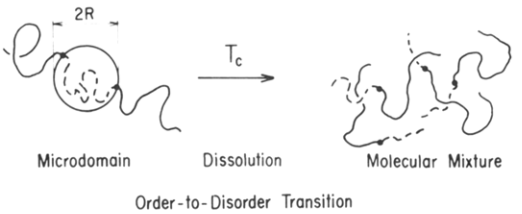

Figure 3. Schematic diagram showing order-to-disorder transition at critical temperature T_c. At $T < T_c$, the microdomains exist in the solution, which gives rise to an ordered arrangement of the polymers in the solution, while at $T > T_c$ the microdomains are dissolved into a more or less homogeneous molecular mixture, which gives rise to a disordered, isotropic arrangement of the polymers in the solution.

III. SAXS Studies on Ordered Structures in Solution

Figure 1 shows oscilloscope displays of the uncorrected SAXS profiles from the block polymer solutions at various concentrations during heating (top row) and cooling processes (bottom row). The origin of each profile was shifted diagonally to avoid overlap. The white arrows in the figure indicate the scattering maxima attributed to interparticle interference, their relative angular positions being located at $\sqrt{1}$, $\sqrt{2}$, and $\sqrt{3}$. Quantitative investigations of the desmeared scattering profiles together with volume consideration revealed that the spherical microdomains composed of PS chains are dispersed in the matrix of PB solutions in a simple cubiclike lattice at low temperatues.[1]

With increasing temperature the lattice tends to be disordered at a relatively narrow temperature range, defined as the *lattice-disordering* temperature, resulting in a sudden increase of the line profiles of the first-order peak (see Figure 4) and an overlap or extinction of the second- and third-order peaks at $\sqrt{2}$ and $\sqrt{3}$, respectively. The lattice-disordering phenomenon may be seen at temperatures between 50 and 60 °C for an 11 wt % solution, between 60 and 70 °C for a 20 wt % solution, between 80 and 90 °C for a 35 wt % solution, and between 100 and 140 °C for a 60 wt % solution in Figure 1. Figure 2 schematically illustrates the lattice-disordering phenomenon. Above the lattice-disordering temperatures, the long-range spatial order of the spherical microdomains are lost, while the nearest-neighbor distance of the domains (i.e., the short-range order) is preserved.

Upon a further increase of temperature the first-order scattering maximum itself disappears, or its peak intensity becomes extremely weak at critical temperature T_c. The extinction of the first-order peak is attributed to an order-to-disorder transition that invokes a dissolution of the microdomain structure into, more or less, a homogeneous mixture of PS and PB chains at the molecular level as schematically illustrated in Figure 3.

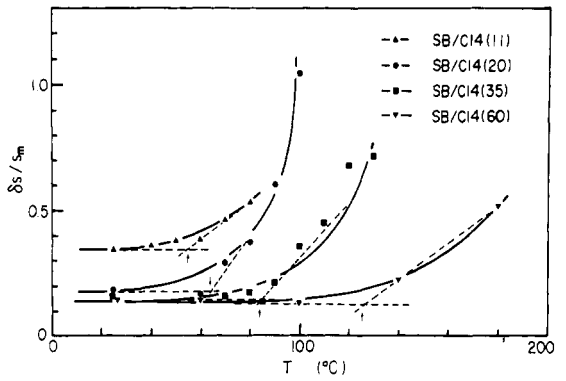

Figure 4. Temperature dependence of the full width at half-maximum (fwhm) of the SAXS profiles at the first-order scattering maximum for the SB solutions at various concentrations. In the code SB/C14(x), x refers to the weight percent of the SB block polymer in n-tetradecane C14. The arrows indicate the lattice disordering temperature T_d.

The thermal transition temperatures T_d and T_c are obviously a function of concentration, i.e., the higher the concentration the higher the temperatures (see Figures 1 and 7). It is also shown in Figure 1 that the change of the SAXS profile with temperature is essentially reversible, indicating that the microdomain structure in our system, including the short-range and long-range spatial orders of the spherical domains, closely follows thermal equilibrium.

1. Lattice-Disordering Phenomenon. In order to investigate the lattice-disordering phenomenon, SAXS profiles were measured at finer temperature intervals than those in Figure 1 and were corrected for absorption, parasitic scattering, scattering from the cell enclosing the solution, background scattering arising from the thermal diffuse scattering, collimation errors in both slit-width and slit-length directions, and nonuniformity of the detector sensitivity of the PSPC as indicated in the previous paper.[1] From the first-order scattering maximum (at the reduced scattering angle s_m) of the corrected scattering profiles (which were shown in the previous paper[1]), the Bragg spacing D and the full width at half-maximum (fwhm) δs were estimated:

$$Ds_m = 1 \qquad s_m = (2 \sin \theta_m)/\lambda \tag{1}$$

where $2\theta_m$ and λ are the scattering angle of the first-order maximum and X-ray wavelength, respectively.

Figure 4 shows the temperature dependence of the fwhm $\delta s/s_m$. The lattice-disordering temperature T_d is defined as shown by the arrows in the figure, i.e., as an inflection point of $\delta s/s_m$ plotted vs. T. It is clearly shown that at a given concentration the line profile is unaltered below T_d but becomes increasingly broader above T_d: at a given temperature, the higher the concentration, the smaller the value $\delta s/s_m$ and therefore the smaller the lattice disorders.

At this point let us discuss the nature of the quasi-elastic force responsible for this superlattice below T_d, keeping in mind all the experimental evidence given above. In our system this force originates from the conformational entropy of the PB block chains emanating from the spherical microdomains composed of the PS block chains.[4] That is, when the interdomain distance D_0 becomes too large, it tends to create a density deficiency of the PB segments toward the center of the matrix. This density deficiency may be compensated either (i) by an excess amount of solvent molecules in the center of the matrix to keep overall segmental density constant[5] or (ii) by stretching the PB chains to fill the space in the center of the domains. In both cases the free energy of the system $G(D_0; \phi_P, T)$ (ϕ_P is the polymer volume fraction) increases with increasing interdomain distance D_0 due either to increasing concentration gradient of the PB segments (case i) or to increasing loss of the conformational entropy (case ii). Thus in this case an attractive force F is exerted between the particles to decrease the free energy of the microdomain system ΔG by decreasing D_0.

If the two PS domains come too close to each other, the volume available to the PB segments becomes too small, resulting in a loss of conformational entropy. Thus in this case a repulsive force F acts on the particles to decrease ΔG by increasing D_0. The equilibrium value of D_0 (D_{eq}) is determined so as to minimize ΔG with D_0.[30]

At high concentrations, the osmotic compressibility of the solution becomes low.[6-8] Consequently, the conformational entropy of the PB chains determines stability of the superlattice. The higher the concentration, the deeper is the free-energy well with D_0 around D_{eq} and the greater is the quasi-elastic restoring force $f(\phi_P,T)$ for a unit displacement of D_0, resulting in the greater stability of the lattice:

$$f(\phi_P,T) = \left[\frac{\partial F(\phi_P,T)}{\partial D_0}\right]_{\phi_P,T} = \left[\frac{\partial^2 \Delta G(D_0;\phi_P,T)}{\partial D_0^2}\right]_{D_0=D_{eq},\phi_P,T} \tag{2}$$

$$\left[\frac{\partial \Delta G(D_0;\phi_P,T)}{\partial D_0}\right]_{D_0=D_{eq},\phi_P,T} = 0 \tag{3}$$

where $F(\phi_P,T)$ is the quasi-elastic restoring force.

If the spherical domains are in the field of the quasi-elastic force with a "spring constant" $f(\phi_P,T)$, then the distribution of the interparticle distance D_0 is given by a Gaussian function with a variance σ_d^2 given, from Boltzmann's law, by[9]

$$\sigma_d^2(\phi_P,T) = k_B T/f(\phi_P,T) \tag{4}$$

where k_B is Boltzmann's constant. If the origin of the quasi-elastic force is the conformational entropy of the PB chains, then

$$f(\phi_P,T) \sim k_B T \tag{5}$$

Therefore, $\sigma_d^2(\phi_P,T)$ is independent of temperature, and consequently the fwhm $\delta s/s_m$ is also almost independent of temperature, as shown in Figure 4 at $T < T_d$ (see eq 29).

If the origin of the quasi-elastic force is energetic, $f(\phi_P,T)$ is essentially independent of T. Consequently

$$\sigma_d^2 \sim T \tag{4a}$$

which might be a possible reason why σ_d^2 or $\delta s/s_m$ increases with temperature at $T > T_d$. The above argument is not directly applicable to our case even at $T > T_d$, since $f(\phi_P,T)$ is primarily entropic but not energetic. However, we may speculate that the increase of σ_d^2 or $\delta s/s_m$ with temperature at $T > T_d$ is a consequence of increasing energetic contribution to $f(\phi_P,T)$. Due to the increase of energetic contribution to $f(\phi_P,T)$, $f(\phi_P,T)$ may have a weaker temperature dependence than that predicted by eq 5, which in turn results in the effect that the thermal energy $k_B T$ (on the σ_d^2 and $\delta s/s_m$) outweighs the effect of the elastic restoring force constant $f(\phi_P,T)$.

The energetic contribution to $f(\phi_P,T)$ at $T > T_d$ may be envisioned as follows (see Figure 5). Let us consider a case when an intersphere distance is increased from D_{eq} to $D_{eq} + \Delta D$ as in Figure 5a. The free energy of the system would increase with the fluctuation ΔD, because the fluctuation creates a density dip in the region between the two particles or the fluctuation forces the molecules to take the more stretched out conformations to fill the density dip, which results in a loss of conformational entropy. If the

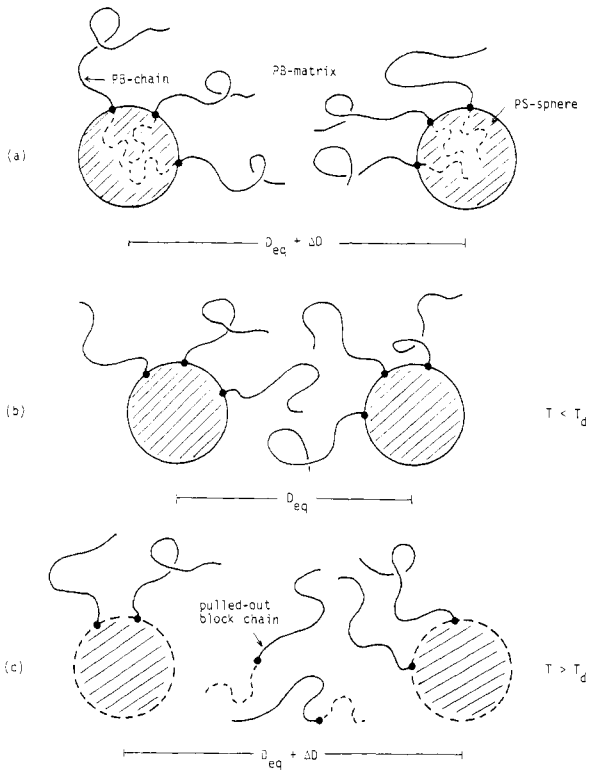

Figure 5. Schematic diagrams showing the lattice disorders. At $T < T_d$, the polybutadiene (PB) chains are firmly anchored to the polystyrene (PS) spheres, so that the quasi-elastic restoring force constant $f(\phi_P,T)$ is proportional to k_BT, while at $T > T_d$ the anchoring of the PB chains is loosened, resulting in some of the block chains being pulled out from the PS spheres and filling in the region between the PS spheres, or resulting in activation of motion of the chemical junction points normal to the interfaces, which stabilizes the fluctuation ΔD.

PB chains are tightly anchored to the PS spheres, the excess free energy can be released only by decreasing the fluctuation ΔD. This is the molecular origin of the attractive force between the spheres, and in this case $f(\phi_P,T)$ is given by eq 5. At $T < T_d$, the PS spheres are unswollen with the solvents because of a high χ value between the solvent and the PS block. Hence the PB chains are firmly anchored to the PS spheres. With increasing temperature the χ value decreases, and hence the spheres are softened. The excess free energy due to the fluctuation ΔD may then be released by pulling out some of the block chains from the spheres and then filling in the density dip with them (see Figure 5c). The pulled-out PS block chains involve thermodynamic interaction with the PB matrix, which however, is a decreasing function of temperature. Thus at $T > T_d$, the fluctuation of the intersphere distance may be stabilized by the *pulling-out and filling-in* mechanism of the block chains, which in turn are stabilized by decreasing thermodynamic interaction between polystyrene and polybutadiene block chains and enhanced by decreasing thermodynamic interaction between solvent and polystyrene block. This may be the molecular origin of the energy contribution to $f(\phi_P,T)$.

Equation 5 may be generalized as follows:

$$f(\phi_P,T) \sim N_{eff}k_BT \tag{5a}$$

where N_{eff} is the number of active polybutadiene block chains that are firmly anchored to the polystyrene spheres and contribute to elastic restoring force. The value N_{eff} is generally a function of T. At $T < T_d$, N_{eff} is independent of temperature, while at $T > T_d$, N_{eff} is a decreasing function of T due to the pulling-out and filling-in mechanism, resulting in $f(\phi_P,T) \sim T^n$ $(n < 1)$.[31]

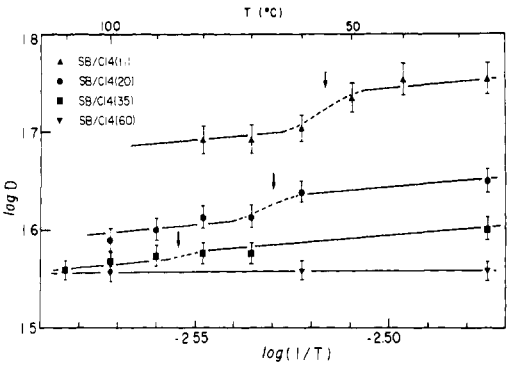

Figure 6. Temperature dependence of the Bragg spacing D estimated from the first-order SAXS maximum for the SB solutions at various concentrations. The discontinuity of D with T as shown in the arrows is a consequence of the lattice-disordering phenomenon.

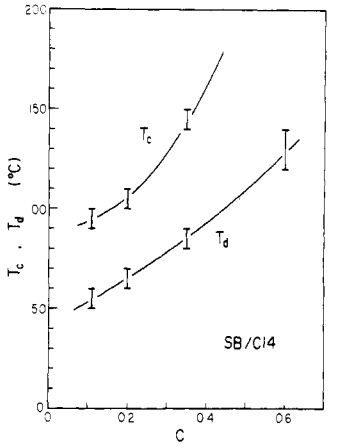

Figure 7. Variations of T_c and T_d as a function of C, the weight fraction of polymer in the solution.

Another consequence of the lattice disordering is seen in the *discontinuous* change of the Bragg spacing D when the temperature is changed across T_d. This is shown in Figure 6, where log D is plotted with log $(1/T)$. As discussed in detail in the previous paper, at $T < T_d$ the microdomains are arranged in a simple cubic lattice. Consequently the Bragg spacing D has a definite physical meaning and is identical with D_0, the nearest-neighbor distance, and the length of the cell edge a_{sc} for the simple-cubic lattice. However, at $T > T_d$ the long-range order of the domains is lost. Consequently, one cannot apply Bragg's law to the SAXS maximum from the disordered structure having the short-range order only. In other words, the Bragg spacing D estimated from eq 1 does not have a well-defined physical meaning. Thus discontinuous change of D with T is an artifact caused by an erroneous application of Bragg's law for the disordered structure above T_d. This point is further analyzed in section III-3.

The temperature dependence of D follows a power law as described in the previous paper:

$$D \sim (1/T)^{\sim 1/3} \tag{6}$$

which may be interpreted as a consequence of decreasing segregation power of the PB and PS chains with temperature.[1]

2. Order-to-Disorder Transition. Figure 7 shows the concentration dependence of the critical temperature T_c where the order-to-disorder transition occurs, as well as that of the lattice-disordering temperature T_d. The quantity C is the weight fraction of polymer in the solution.

Below T_c the chemical junction points of the block polymers are restricted in a relatively narrow interfacial

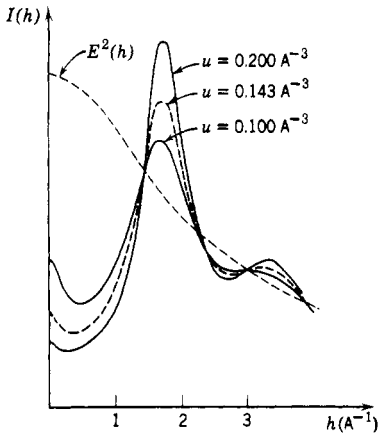

Figure 8. Scattering profiles $I(h)$ of liquid argon at three reduced densities u and the particle scattering intensity $E^2(h)$. $h = (4\pi/\lambda) \sin\theta$, and 2θ is the scattering angle (Guinier and Fournet[17]). From the angular position of the scattering maximum, h_{max}, one can estimate the "apparent" Bragg spacing D for the liquid state.

region. Moreover, the end-to-end vectors of the block chains are preferentially oriented normal to the interface, giving rise to a kind of mesomorphic, ordered structure. On the other hand, above T_c the chemical junction points are distributed randomly in three-dimensional space, and the end-to-end vectors also orient randomly in space, giving rise to an isotropic, disordered structure. The higher the concentration, the higher is the critical temperature T_c, which may be interpreted as a consequence of increasing effective segregation power between the PS and PB chains with increasing C.

3. SAXS Analyses on the Discontinuity of Bragg Spacing D with T at T_d. We analyze here the discontinuous decrease of the "apparent" Bragg spacing D with increasing T above T_d. In order to simplify the analysis, we consider a model system in which an assembly of simple particles (like argon) at a given particle density (ϕ_P) undergoes a thermal transition corresponding to the lattice disordering of the spherical domains, i.e., the transition in the spatial arrangement of the particles from a simple-cubic lattice to liquid. We estimate the "apparent" Bragg spacing D by applying eq 1 to the SAXS maximum from the liquid state, the value of which is then compared with the spacing D, identical with the cell edge a_{sc}, estimated for the system with a simple-cubic lattice.

The scattering from the simple liquid composed of spherically symmetric particles may be given by[14,15]

$$I(h) = I_e(h)\bar{N}_v E^2(h)[1 - ((2\pi)^{3/2}\epsilon/v_1)\beta(h)]^{-1} \quad (7)$$

where $h = 2\pi s = (4\pi/\lambda) \sin\theta$ (2θ being the scattering angle), $E^2(h)$ is the scattering intensity from a single particle, $I_e(h)$ is the Thomson scattering from an electron, $\bar{N}_v$ is the average number of particles in the irradiated volume, v_1 is the volume occupied by a particle, and ϵ designates a constant approximately equal to unity. The function $\beta(h)$ is given by

$$h\beta(h) = (2/\pi)^{1/2} \int_0^\infty r\alpha(r) \sin hr \, dr \quad (8)$$

with

$$\alpha(r) = \exp[-\Phi(r)/k_B T] - 1 \quad (9)$$

where $\Phi(r)$ is the potential energy of a pair of particles whose centers are separated by a distance r.

Fournet has derived eq 7 on the basis of the Born and Green theory on equation of state[16] and has employed eq 7 to predict the scattering by liquid argon of several densities u, some results of which are shown in Figure 8.[17] We

Table I
h_{max} and the Apparent Bragg Spacing (D) of the Liquid Argon and the Corresponding Cell Edge (a_{sc}) of the Simple-Cubic Lattice as a Function of Density (u) or Fractional Volume of Argon (ϕ_P)

u, Å^{-3} [a]	ϕ_P	h_{max}, Å^{-1} [b]	D, Å [c]	a_{sc}, Å [d]	a_{sc}/D
0.100	0.185	1.675	3.75	5.40	1.43
0.143	0.265	1.716	3.66	4.79	1.31
0.200	0.371	1.736	3.62	4.29	1.18

[a] $u = (2\pi)^{3/2}/v_1^*$, $v_1^* = v_1/\epsilon$. [b] Estimated from Figure 8. [c] Estimated by applying Bragg's law for the SAXS maximum from the liquid, $D = 2\pi/h_{max}$. [d] Estimated from eq 12 by assuming a simple-cubic lattice.

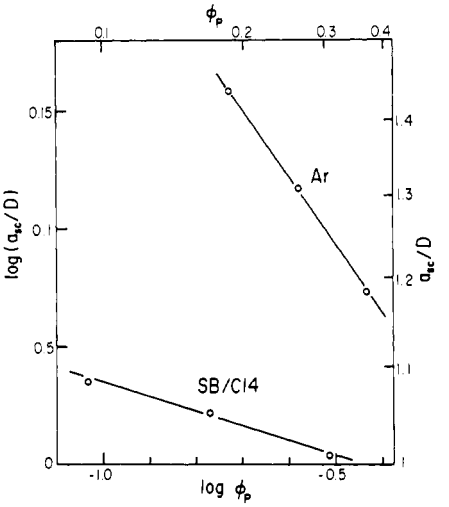

Figure 9. The ratio of the Bragg spacing for the superlattice (identical with the cell edge a_{sc} in the case of a simple-cubic lattice) to the "apparent" Bragg spacing D for the liquid state for n-tetradecane solution of the SB block polymer and for argon. Note that the discontinuity of the Bragg spacing involved by the lattice disordering (a_{sc}/D) increases with decreasing particle volume fraction for argon or polymer volume fraction.

may apply Bragg's law to the scattering maximum from the liquid to obtain the "apparent" Bragg spacing $D = 2\pi/h_{max}$ (h_{max} being the value h that gives rise to the scattering maximum) as a function of the densities u or the volume fractions of the particle ϕ_P as defined by

$$u \equiv (2\pi)^{3/2}/v_1^* \quad (10a)$$

$$\phi_P = v_0/v_1^* \qquad v_1^* = v_1/\epsilon \quad (10b)$$

where v_0 is the volume of argon. The results are summarized in Table I.

One can estimate also the cell edge a_{sc} as a function of u or ϕ_P if the system hypothetically forms a simple-cubic lattice:

$$\phi_P = \frac{4\pi}{3}\left(\frac{R}{a_{sc}}\right)^3 \quad (11)$$

where R is radius of the particle. From eq 10a, 10b, and 11, it follows that

$$a_{sc} = (2\pi)^{1/2}/u^{1/3} \quad (12)$$

One can estimate the change of Bragg spacing from a_{sc} to D accompanied by the transition in the spatial arrangement of the simple particles from simple-cubic lattice to the liquid state, as a function of concentration as shown in Table I and Figure 9.

As clearly seen in Table I and Figure 9, the structure transition involved by the lattice disordering results in a

Table II
Shear Moduli (G), Yield Stress (σ_0), and Plastic Viscosity (η) at Room Temperature Estimated from the Best Fits with the Experimental Data and the Data Calculated from Eq 13

	concentration C						
parameters	0.11	0.20	0.30	0.35	0.40	0.50	0.60
G, dyn/cm^2	4.4×10^3	9.6×10^3	1.5×10^4	1.7×10^4	1.7×10^4	2.8×10^4	3.4×10^4
σ_0, dyn/cm^2	1.0×10^2	4.0×10^2	6.0×10^2	1.0×10^3			
η, P	5.0×10^1	8.0×10^2	4.5×10^3	2.0×10^4			

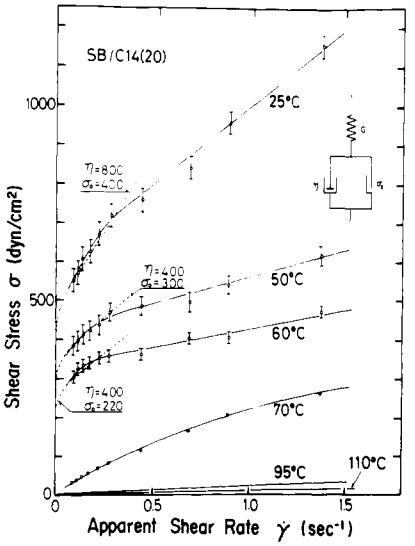

Figure 10. Steady-state flow behavior of 20 wt % n-tetradecane solution at relatively low shear rates at various temperatures. The broken lines indicate simulated curves with the constitutive equation (13) for a given set of the parameters η and σ_0.

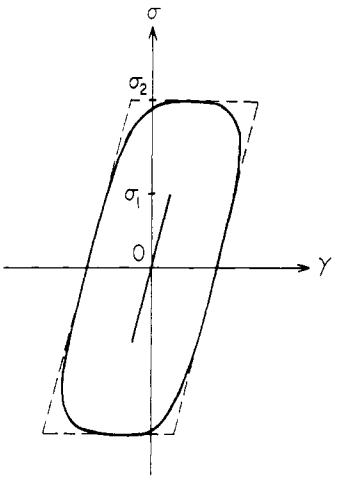

Figure 11. Schematic representation of the Lissajou's patterns of SB/C14 system below and above the yield stress σ_0 ($\sigma_1 < \sigma_0 < \sigma_2$).

discontinuous decrease of the Bragg spacing from a_{sc} to D. The discontinuity of the spacing is a function of concentration: the greater the concentration, the smaller the discontinuity. The general trend is exactly parallel to that observed in the microdomain system of the block polymer solution, which confirms our speculation on the discontinuity of the Bragg spacing involved by the lattice disordering.

IV. Rheological Behavior

In this section we shall discuss the effects of the two transitions, the lattice disordering and the order-to-disorder transition, on the rheological properties of the block polymer solution. The transitions will be induced thermally at T_d and T_c as described in sections III-1 and III-2 at a given concentration or by changing concentrations at C_d and C_c at a given temperature (C_d and C_c corresponding to the concentrations where the lattice disordering and the order-to-disorder transition occur, respectively). The detailed analysis of the rheological behavior itself was described thoroughly in a previous paper.[3]

1. Change of Rheological Behaviors at T_d and T_c. Figure 10 shows typical results of the temperature dependence of the steady-state flow behavior of the 20 wt % n-tetradecane solution at a relatively low shear rate. The solid lines are the measured curves, while the broken lines are calculated results based on the constitutive equation for the mechanical model as shown also in Figure 10, where σ_0 is the yield stress, η is the plastic viscosity, and G is the shear modulus:

$$u(\sigma - \sigma_0)\frac{\sigma - \sigma_0}{\eta} + u(-\sigma - \sigma_0)\frac{\sigma + \sigma_0}{\eta} + \frac{\dot{\sigma}}{G} = \dot{\gamma} \quad (13)$$

with

$$u(x) = 1 \quad \text{for } x > 0 \qquad u(x) = 0 \quad \text{otherwise} \quad (14)$$

The values σ_0 and η given in the figure give the best fit to the experimental results.[3]

For a better assessment of σ_0, we also utilized the results of dynamic measurements. Figure 11 shows schematically a typical Lissajou's pattern of the system below and above the yield stress σ_0. The system exhibits *linear elasticity* (rectilinear Lissajou's pattern with maximum stress σ_1 and loss tangent less than 0.1) at the stress level below σ_0 and *nonlinear* viscoelastoplasticity at the stress level above σ_0 (lozenge-shaped pattern with maximum stress σ_2). Such experiments lead to $\sigma_1 < \sigma_0 < \sigma_2$, and by decreasing the range $\sigma_2 - \sigma_1$, one can determine σ_0. The results shown in Table II are thus obtained by simultaneously considering the best fit of the steady-state flow curve with the constitutive equation and the linear and nonlinear criteria of the dynamic response.

The results in Figure 10 show that the solution apparently exhibits a yield stress σ_0 at low temperatures (below 60 °C). The value decreases with increasing temperature and vanishes at temperatures higher than 70 °C. The lattice disordering temperature T_d of this solution is about 65 °C from Figure 4 and Figures 6 and 7. Thus the solution has a finite apparent yield stress at temperatures below T_d where the superlattice exists but no yield stress at temperatures above T_d. The apparent yield stress corresponds to the mechanical energy imposed on the solution that is dissipated to destroy the superlattice. The dynamic test shows that below T_d the solution exhibits linear elasticity if the shear stress is lower than σ_0 and nonlinear plasticity if the shear stress is higher than σ_0. As temperature is increased above T_d, the solution exhibits a transition in rheological behavior from nonlinear, plastic flow to linear, non-Newtonian flow.

Upon further increase of temperatures, the flow changes from linear, non-Newtonian to linear, Newtonian behavior, as is also seen from Figure 10, at a temperature corresponding approximately to T_c ($\simeq$105 °C) for the order-to-disorder transition. This mechanism of the rheological transition at higher temperature has been proposed by a

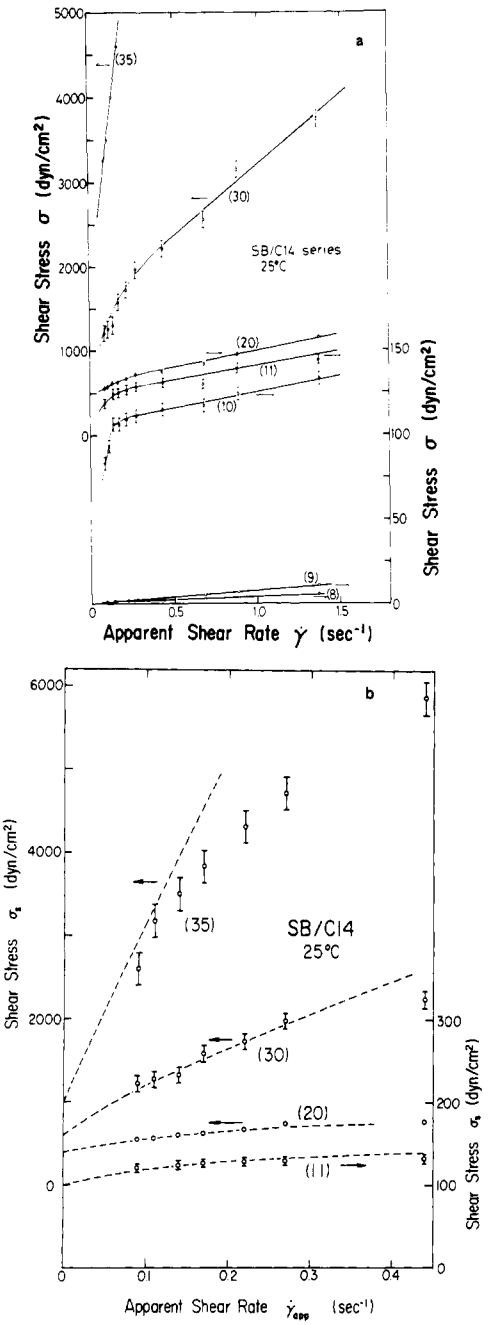

Figure 12. (a) Steady-state flow behavior of *n*-tetradecane solutions at 25 °C at various concentrations: 8, 9, 10, 11, 20, 30, and 35 wt %. (b) Simulation of the experimental data (open circles) at low shear-rate region with the constitutive equation (13) for the given set of the parameters shown in Table II.

number of workers[18-24] and confirmed unequivocally by means of simultaneous measurements of SAXS.[3,25,26]

2. Concentration Dependence of Rheological Behavior. Figure 12a shows typical results of the concentration dependence of the steady-state flow behavior of the *n*-tetradecane solution at a relatively low shear rate at 25 °C. It is shown in the previous paper[1] that the spherical microdomains themselves exist in the solutions with concentrations greater than 8 wt %. That is, the critical concentration C_c where the order-to-disorder transition occurs is approximately equal to or less than 8 wt %. It is also shown that at 11 wt % the solution clearly possesses the long-range spatial order of the spherical microdomains but that at 8 wt % the solution does not, since it does not show well-defined higher order maxima. Thus the concentration C_d at which the lattice disordering occurs exists

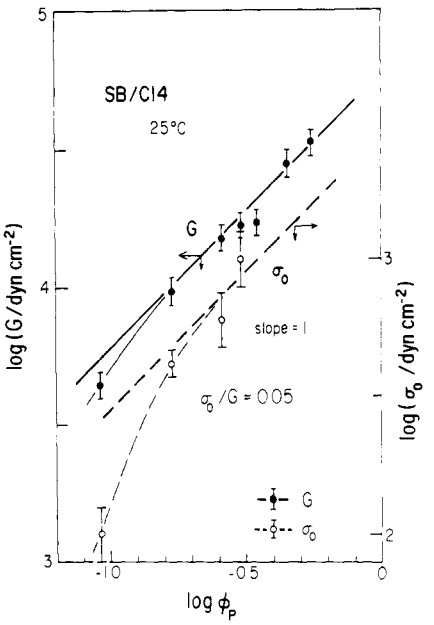

Figure 13. Concentration dependence of the yield stress σ_0 (open circles and dashed lines) and shear modulus G (solid circles and solid lines) for the *n*-tetradecane solution of the SB block polymer at 25 °C. At high concentrations $\phi_P \gtrsim 0.2$; G and σ_0 linearly vary with ϕ_P.

in the range of $0.8 < C_d < 0.11$ from the SAXS studies.[1]

The solutions with concentrations greater than C_d have the apparent yield stress σ_0: the higher the concentration, the larger the σ_0. As the concentration decreases below C_d, the rheological behavior changes from nonlinear, plastic flow to linear, non-Newtonian flow. The latter flow behavior should further change to linear, Newtonian flow with a further decrease of the concentration below C_c, which is, however, far below the lowest concentration that can be tested in these rheology measurements.

The data obtained at shear rates lower than 0.5 in Figure 12a were analyzed in terms of the constitutive equation (13). The results of the best fits with the experimental data (open circles) are shown in Figure 12b with broken lines. The parameters σ_0 and η thus estimated are listed in Table II. The parameter G also was measured from dynamic measurements in the linear elastic region of $\sigma < \sigma_0$. As shown in Figure 13, the apparent yield stress σ_0 as well as G varies approximately linearly with ϕ_P (having a slope of unity in the double-logarithmic plot) well above the critical volume concentration of polymer ϕ_d at which the superlattice is formed in the solution. As ϕ_P approaches ϕ_d, the values σ_0 and G decrease to zero:

$$\sigma_0 \sim \phi_P \qquad G \sim \phi_P \qquad \text{for } \phi_P \gg \phi_d \tag{15a}$$

$$\sigma_0 \to 0 \qquad G \to 0 \qquad \text{for } \phi_P \to \phi_d \tag{15b}$$

From the figure the yield strain $\gamma_y \equiv \sigma_0/G$ is estimated to be about 0.05. We shall give a qualitative interpretation of eq 15a below.

Free energy of the microdomain formation ΔG from the disordered molecular mixture of the PS and PB chains and solvents may be given by

$$\Delta G = \Delta H_{int} - T\Delta S_p - T\Delta S_{constr} + \Delta G_{mix} \tag{16}$$

where ΔG_{mix} is the free energy of demixing of the PS and PB chains, and the solvents (e.g., demixing of the solvent from the spherical domains composed of the PS chains), ΔH_{int} is heat of mixing of the PS and PB chains and the solvents in the interfacial region, ΔS_p is the loss of entropy involved by confining the junction points of the block

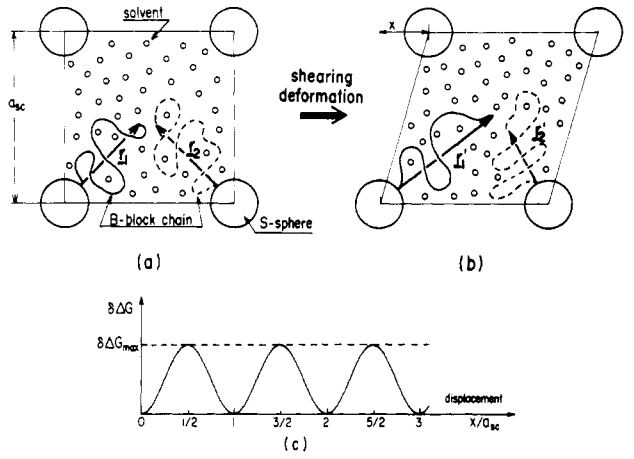

Figure 14. Schematic diagram showing the elastic deformations of the PB block chains with its end-to-end vectors from ($\mathbf{r}_1$, $\mathbf{r}_2$) (a) to ($\mathbf{r}_1'$, $\mathbf{r}_2'$) (b) accompanied by the shear deformation and (c) that showing the free-enegy change $\delta\Delta G$ accompanied by the relative displacement of the particles in the upper layer with respect to the lower layer (x/a_{sc}), without involving any heat-dissipation mechanisms.

polymers in the interfacial region, and ΔS_{constr} is the constraint entropy, which is a loss of entropy involved by confining the respective chains in the respective domain space while keeping the demand of uniform space-filling with the segments.[10-12]

When the shear deformation is applied to the lattice, as may be depicted in Figure 14, the change of free energy $\delta\Delta G$, at the high concentration regime may be given by

$$\delta\Delta G = \delta\Delta H_{int} - T\delta\Delta S_p - T\delta\Delta S_{constr} + \delta\Delta G_{mix} \simeq -T\delta\Delta S_{constr} \quad (17)$$

This is because the shear deformation may not involve significant change either in the spatial, segmental density distributions of the block chains and the solvent molecules in the interphase (leading to $\delta\Delta H_{int} \simeq 0$) or in the interfacial volume fraction (leading to $\delta\Delta S_p \simeq 0$). Also, the shear deformation may not involve significant changes in the partition of the solvents to each phase, leading to $\delta\Delta G_{mix} \simeq 0$. The assumptions made above may be legitimate when the concentration is relatively high and the osmotic compressibility becomes low enough to suppress the concentration fluctuations.

The change of the constraint entropy $\delta\Delta S_{constr}$ may be given by

$$\delta\Delta S_{constr} = Nk_B \ln (P_{constr}/P^0_{constr}) \quad (18)$$

where N is the total number of the chains in the system, P^0_{constr} is the probability density of the PB chain with all the segments being confined in the matrix phase while satisfying the requirement of the uniform space-filling with the PB segments, and P_{constr} is the corresponding probability density of the PB chain for the deformed state.

The root mean square end-to-end distance (rms) of the PB chains is determined from the demand of the uniform filling of the space with segments. When the simple-cubic lattice is deformed by the shear stress, the end-to-end vectors $\mathbf{r}_1$ and $\mathbf{r}_2$ are deformed to $\mathbf{r}_1'$ and $\mathbf{r}_2'$, respectively, to satisfy the demand of the uniform filling even in the deformed state (Figure 14). The elastic deformation of the polymer coils that leads to stretching of the rms of one type of chains ($\mathbf{r}_1 \rightarrow \mathbf{r}_1'$) and to compressing of the rms of the other type of chains ($\mathbf{r}_2 \rightarrow \mathbf{r}_2'$) results in a decrease of the probability density from P^0_{constr} to P_{constr} leading to a decrease of the constraint entropy term $\delta\Delta S_{constr}$ and consequently increase of the free energy $\delta\Delta G$:

$$\delta\Delta G \simeq Nk_BT \ln (P^0_{constr}/P_{constr}) \quad (19)$$

The variation of $\delta\Delta G$ with shear strain γ may be calculated in terms of the confined chain statistics subjected to the shear deformation.

If the particles in the upper layer in Figure 14 are displaced by x/a_{sc} relative to those in the lower layer by the shear deformation without involving any heat-dissipation mechanisms, $\delta\Delta G$ should periodically vary with x/a_{sc} as shown in Figure 14c. The shear modulus G may be then calculated as

$$\delta\Delta G = \sigma\gamma V = G\gamma^2 V$$

Hence

$$G = (\delta\Delta G/V)/\gamma^2 \quad (20)$$

where V is the volume of the system and γ is the shear strain (x/a_{sc}). From eq 19 and 20 it follows that

$$G = \left(\frac{N}{V}\right)\frac{k_BT}{\gamma^2} \ln (P^0_{constr}/P_{constr}) \quad (21)$$

$$G \sim N/V \sim \phi_P \quad (22)$$

Therefore G is proportional to polymer volume concentration ϕ_P, leading to eq 15a. We shall later discuss eq 22.

Moreover we assume that the periodic function of $\delta\Delta G(x)$ may be given by

$$\delta\Delta G(x) = \delta\Delta G_{max} \sin^2 (\pi x/a_{sc}) \quad (23)$$

where $\delta\Delta G_{max}$ is the free-energy barrier that must be overcome for the system to flow. That is, if the applied mechanical energy is smaller than a critical value proportional to $\delta\Delta G_{max}$, the energy is stored in the lattice and recoverable. However, if the applied energy exceeds the critical value, it is not stored in the lattice but is dissipated as heat. The stress σ_{max} corresponding to $\delta\Delta G_{max}$ imposed to the system to jump the barrier is assumed to be proportional to the yield stress σ_0. Then the force $F(x)$ exerted on a given particle by the particles in the neighboring lattice is given from

$$F(x) = -\partial\delta\Delta G(x)/\partial x = F_{max} \sin (2\pi x/a_{sc}) \quad (24)$$

The shear stress σ is then given by

$$\sigma(x) = N_S F_{max} \sin (2\pi\gamma) \quad (25)$$

where N_S is the number of particles per unit area and $N_S F_{max}$ can be interrelated to G

$$G = (d\sigma/d\gamma)_{\gamma=0} = 2\pi N_S F_{max} \quad (26)$$

Thus from eq 22 and 26

$$\sigma = (G/2\pi) \sin (2\pi\gamma) \quad (27)$$

$$\sigma_{max} = G/2\pi$$

Consequently, from eq 22 and 27

$$\sigma_0 \sim G \sim \phi_P \quad (28)$$

Equation 28 explains why σ_0 and G have the same power law for the concentration dependence as shown in Figure 12. The basic assumption $\sigma_{max} \sim \sigma_0$ remains unproven here, and the assumption involved in eq 23 or the accuracy of the equation has to be discussed on the basis of detailed statistical mechanical considerations.

Now coming back to eq 21 and 22, P^0_{constr} and P_{constr} themselves are strong functions of ϕ_P but the ratio P_{constr}/P^0_{constr} may be just a weak function of ϕ_P, depending primarily on a weak concentration dependence of the statistical segment length. Consequently we assumed that

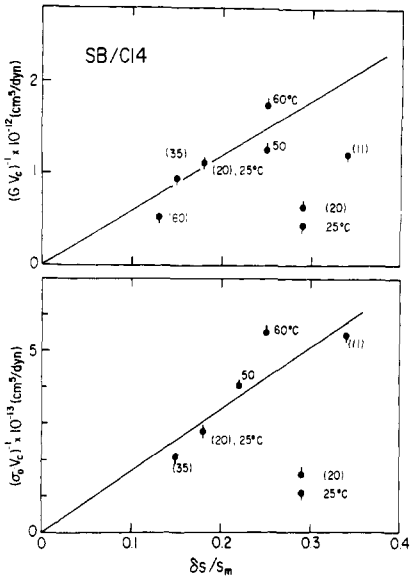

Figure 15. A master relationship between $\delta s/s_m$ and $(GV_c)^{-1}$ or $(\sigma_0 V_c)^{-1}$ obtained from the measurements of concentration dependence at 25 °C (numbers in parentheses represent the concentration C in weight percent of polymers) and of temperature dependence at 20 wt % concentration (numbers without parentheses represent the temperature).

$\ln (P^0_{constr}/P_{constr})$ is independent of ϕ_P for our qualitative treatment, which leads to eq 22 and 28.

3. Interrelation between the Structural and Rheological Parameters. In this section we shall discuss an interrelation between the structural parameters such as a_{sc} and $\delta s/s_m$ and the rheological parameters such as G and σ_0 in the high-concentration and low-temperature regime where the superlattice exists.

According to the scattering theory from the ideal paracrystal[27] with the small lattice disorder σ_d, $\delta s/s_m$ is given by

$$\delta s/s_m \simeq \pi^{3/2}(4 \ln 2)^{1/2}(\sigma_d/a_{sc})^2 \quad (29)$$

where σ_d is the standard deviation of the nearest interparticle distance from the average value a_{sc}. For simplicity, the lattice is assumed to have isotropic disorders in eq 4. The distribution of the distance in the field of the quasi-elastic force is given by a Gaussian form with σ_d, which in turn is given by eq 4 and the spring constant f given from eq 24 and 26 by

$$f = \partial F(x)/\partial x|_{x=0} = G/(a_{sc}N_S) \quad (30)$$

Thus from eq 29, 4, and 30 and by noting that $N_S \sim a_{sc}^{-2}$, one obtains

$$\delta s/s_m \sim k_B T/(GV_c) \sim k_B T/(\sigma_0 V_c) \quad (31)$$

where V_c is the unit cell volume of the macrolattice. Thus one expects that $\delta s/s_m$ is linearly proportional to $(GV_c)^{-1}$ or $(\sigma_0 V_c)^{-1}$. The structural and rheological data obtained at the various temperatures and concentrations should fall onto a single master curve given by eq 31.

The preliminary experimental results used to investigate the eq 31 are shown in Figure 15. Although the data points are scattered and limited in number, the results seem to support the relation. From Figure 15 it is also concluded that

$$\sigma_0/G \simeq 0.05 \quad (32)$$

for our system. Thus the yield strain γ_y thus estimated is about 5%, which is far smaller than that for a perfect simple-cubic lattice. Thus the yielding phenomenon observed here is strongly affected by lattice defects.

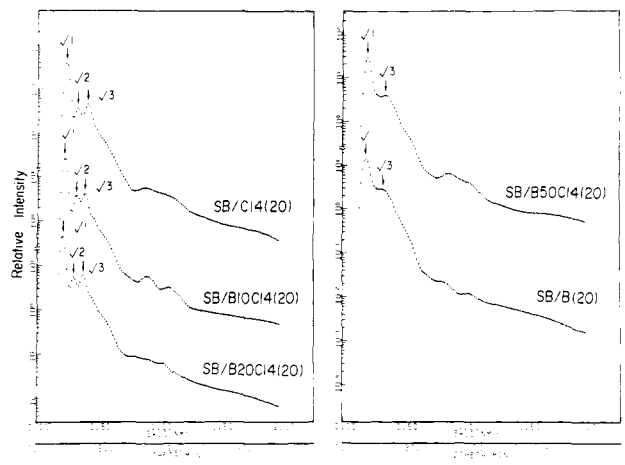

Figure 16. Variations of the desmeared and corrected SAXS profiles of the n-tetradecane solution of the SB block polymers with an addition of homopolybutadiene (HPB). In the code of SB/BxC14(20), 20 designates the weight percent of the SB block in the ternary mixture, and x designates the weight percent of the HPB (B) in the mixture of HPB and n-tetradecane (C14), which form the matrix phase for spherical domains.

V. Effects of Blending Homopolybutadiene on Lattice Disordering and Rheological Behavior

Figure 16 shows the change of the desmeared and corrected SAXS profiles at room temperature with an addition of homopolybutadiene (HPB) ($\bar{M}_n = 2 \times 10^3$) to the solution. The HPB is believed to be solubilized in the matrix of the PB solution. In this series of specimens, the weight fraction of the SB block polymers in the ternary mixture of SB, HPB, and n-tetradecane was always kept at 0.2, while the weight percent x of HPB in the mixture of HPB and n-tetradecane (which forms the matrix phase) was varied systematically from 0 to 100 (0, 10, 20, 50, and 100 wt %). The ternary mixture is coded as SB/BxC-14(20), where 20 designates the weight percent of SB in the ternary mixture and x designates the weight percent of HPB (B) in the mixture of HPB and n-tetradecane (C14).

It is clearly seen that the line profile broadens with increasing HPB content. Three scattering maxima at relative angular positions of $1:\sqrt{2}:\sqrt{3}$ are clearly discernible for the systems with HPB content x less than or equal to 20. Upon further increase of HPB content, the line profile dramatically broadens, and the maxima at $\sqrt{2}$ and $\sqrt{3}$ overlap into a single broad mixima, indicating that the lattice disordering takes place at the HPB content x greater than 20 and close to 50.

The lattice disordering accompanied by the addition of HPB is more quantitatively analyzed in terms of the fwhm $\delta s/s_m$ plotted in Figure 17 as a function of weight fraction of the HPB (w_{HPB}), as a buffer, in the mixture of the PB block chains and the HPB chains. The relative fwhm is almost constant at $w_{HPB} \lesssim 0.59$ (corresponding to $x \lesssim 20$). Upon further increase of the w_{HPB}, it dramatically increases. The lattice disordering occurs at the inflection point $w_{HPB} \simeq 0.66$ (i.e., $x \simeq 27$) as shown by the arrow in the figure.

All these results agree well with the prediction derived from rheological studies by Watanabe et al.[28,29] on SB/C14 solutions mixed with HPB. That is, solutions with HPB content x in the solvent less than 20 exhibit nonlinear and plastic flow, while those with the fraction of HPB more than 50 shows linear viscoelastic behavior (still non-Newtonian at high shear rates). The rheology of these systems strongly suggests that the superlattice formed in the system with $x = 20$ becomes the disordered liquid-like ar-

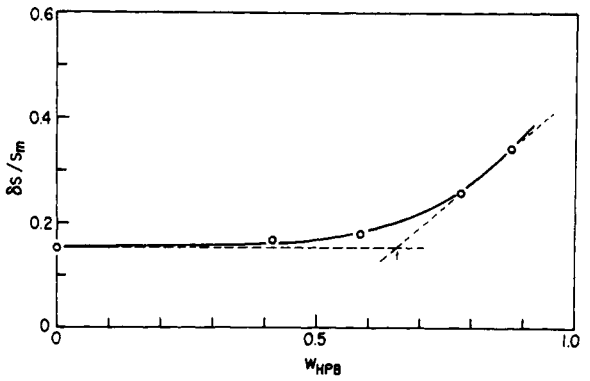

Figure 17. Variations of the fwhm $\delta s/s_m$ with an addition of the homopolybutadiene (HPB) to the *n*-tetradecane solution, SB/BxC14(20). The abscissa w_{HPB} corresponds to the weight fraction of the HPB in the mixture of the HPB and PB chains, i.e., $w_{HPB} = W_{HPB}/(W_{PB} + W_{HPB})$ where W_K is the weight of component K. The lattice disordering takes place at $w_{HPB} \simeq 0.66$ as indicated by the arrow, corresponding to $x \simeq 27$ in the code of SB/BxC14(20).

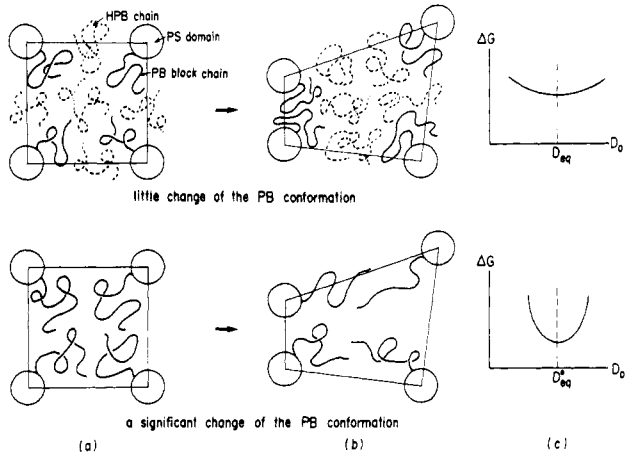

Figure 18. Schematic diagrams showing the effect of addition of homopolybutadiene (HPB) on the lattice disordering. The PB block chains and HPB chains are drawn with solid and broken lines, respectively. In the absence of HPB (the bottom three figures), the lattice disordering from a to b involves a signficant increase of the constraint entropy ΔS_{constr} as a consequence of the elastic deformation of the PB chains to satisfy the demand of the uniform filling of the space with the segments, which gives rise to the big curvature of the free energy ΔG with the interdomain distance D_0 around the equilibrium value D^0_{eq} (c). In the presence of HPB (the upper three figures), the lattice disordering from a to b involves little change of ΔS_{constr} because the density fluctuations of the PB segments can be compensated by the HPB segments, which may give rise to the small curvature of the free energy ΔG with D_0 around the equilibrium D_{eq} (c). Thus the lattice disordering is stabilized by the addition of the HPB.

rangement of the spherical domains when HPB content x is increased to values greater than 50.

The lattice disordering involved by adding the HPB may be understood as follows. In the absence of HPB the density deficiency and excess of PB block chains (solid lines in Figure 18) brought by fluctuations of the interparticle distance should be extinguished by stretching and compressing the polymer coils, resulting in an increase of free energy by a certain amount (see Figure 18, bottom figures). In the presence of the HPB, these fluctuations in the segmental density of the PB block chains may be compensated by the HPB chains (broken lines) without a significant increase in the free energy (see Figure 18, top figures). Therefore the curvature of free energy ΔG with D_0 around the equilibrium D_{eq} or D^0_{eq} is smaller for the systems with HPB than for the system without HPB. In other words, the lattice disordering may be stabilized by the addition of HPB.[32]

The same arguments given above lead to the conclusion that the $\delta\Delta G$ and $\delta\Delta G_{max}$ of the system subjected to the shear deformation decrease with increasing the HPB content, giving rise to decreased values of σ_0 and of G.

Acknowledgment. We express our sincere thanks to Dr. D. J. Meier for his stimulating discussions and enlightening comments. We acknowledge with thanks financial support from the Ministry of Education, Science and Culture, Japan (Monbusho), under Grants 56490013 for the Kyoto University Group (addressed to T.H.) and for the Osaka University Group 347081 (addressed to T.K.). The Kyoto University group acknowledges also partial support from the U.S.–Japan Cooperative Research Program of the National Science Foundation and the Japan Society for the Promotion of Science (addressed to H.K.).

Registry No. SB, 9003-55-8; PB, 9003-17-2.

References and Notes

(1) Shibayama, M.; Hashimoto, T.; Kawai, H. *Macromolecules* **1983**, *16*, 16.
(2) This refers to order and disorder at molecular level. That is, the order in the spatial arrangement of the chemical junction points and the orientation of end-to-end vectors of the block polymer chains exist until the dissolution of the microdomains takes place at T_c. On the other hand the lattice disordering refers to an order-to-disorder transition in the spatial arrangement of the microdomains.
(3) Watanabe, H.; Kotaka, T.; Hashimoto, T.; Shibayama, M.; Kawai, H. *J. Rheol. (N.Y.)* **1982**, *26* (2), 153.
(4) Meier, D. J. *J. Phys. Chem.* **1967**, *71*, 1861.
(5) The overall segmental density refers to the sum of the densities of the solvent molecules and of the PB segments.
(6) See, for example: de Gennes, P. G. "Scaling Concepts in Polymer Physics"; Cornell University Press: Ithaca, NY, 1979.
(7) de Cloizeaux, J. *J. Phys. (Paris)* **1975**, *36*, 1199.
(8) Noda, I.; Kato, N.; Kitano, T.; Nagasawa, M. *Macromolecules* **1981**, *14*, 668.
(9) Prins, J. A. *Naturwissenschaften* **1931**, *19*, 435.
(10) Meier, D. J. In "Block and Graft Copolymers"; Burke, J. J., Weiss, V., Eds.; Syracuse University Press: Syracuse, NY, 1973.
(11) Meier, D. *J. Prepr. Polym. Colloq., Soc. Polym. Sci., Jpn.* **1977**.
(12) Helfand, E.; Wasserman, Z. R. *Macromolecules* **1976**, *9*, 879.
(13) Hong, K. M.; Noolandi, J. *Macromolecules* **1980**, *13*, 964.
(14) Fournet, G. *C. R. Hebd. Seances Acad. Sci.* **1949**, *228*, 1801.
(15) Fournet, G. *Acta Crystallogr.* **1951**, *4*, 293.
(16) Born, M.; Green, H. S. *Proc. R. Soc. (London)* **1946**, *A188*, 10.
(17) Taken from Guinier, A.; Fournet, G. "Small-Angle Scattering of X-rays"; Wiley: New York, 1955; p 49.
(18) Chung, C. I.; Gale, J. C. *J. Polym. Sci., Polym. Phys. Ed.* **1976**, *14*, 1149.
(19) Gouinlock, E. V.; Porter, R. S. *Polym. Eng. Sci.* **1977**, *17*, 534.
(20) Pico, E. R.; Williams, M. C. *Polym. Eng. Sci.* **1977**, *17*, 573.
(21) Chung, C. I.; Lin, M. I. *J. Polym. Sci., Polym. Phys. Ed.* **1978**, *16*, 545.
(22) Chung, C. I.; Griesback, H. L.; Young, L. *J. Polym. Sci., Polym. Phys. Ed.* **1980**, *18*, 1237.
(23) Hashimoto, T.; Tsukahara, Y.; Kawai, H. *J. Polym. Sci., Polym. Lett. Ed.* **1980**, *18*, 585, *Macromolecules* **1981**, *14*, 708.
(24) Hashimoto, T.; Shibayama, M.; Fujimura, M.; Kawai, H. *Mem. Fac. Eng., Kyoto Univ.* **1981**, *43*, 184.
(25) Widmaier, J. M.; Meyer, G. C. *J. Polym. Sci., Polym. Phys. Ed.* **1980**, *18*, 2217.
(26) Kraus, G.; Hashimoto, T. *J. Appl. Polym. Sci.* **1982**, *27*, 1745.
(27) Hosemann, R.; Bagchi, S. N. "Direct Analysis of Diffraction by Matter"; North-Holland: Amsterdam, 1962.
(28) Watanabe, H.; Kotaka, T. *Polym. Prepr. Jpn.* **1981**, *30*, 1962; *J. Rheol. (N.Y.)*, in press.
(29) Watanabe, H.; Kotaka, T.; Shibayama, M.; Hashimoto, T.; Kawai, H. *Rheol. Prepr. Jpn.* **1981**, *29*, 129.
(30) In the case when one of the phases (e.g., the A phase) is in the glassy state (polystyrene microdomains being in the glassy state in our case), the size of the other microdomains (e.g., the B microphase) or interdomain distance is primarily determined by a surface density of the chemical junction points of the block polymers in the interfaces of the microdomains, polymer

volume concentration, and molecular weight of B-block chains.

(31) Another possible mechanism responsible for the lattice disordering may be motion of the chemical junction points of the block polymer chains normal to the interfaces. This motion is frozen at $T < T_d$ but becomes increasingly important with increasing T at $T > T_d$. The enhanced motion of the junction points at $T > T_d$ may result in a partial release of energy stored in the individual chains with the lattice distortions. Consequently, the motion gives rise to an effect similar to decreasing N_{eff} in eq 5a.

(32) It should be noted that the replacement of the solvent, *n*-tetradecane, by HPB causes a contraction of the size of the PB block chains. This contraction of chain dimension of the PB block chains is another important factor associated with the lattice disordering stabilized by the addition of HPB. A more detailed discussion along this line will be given elsewhere.[28]

Effects of Annealing and Prior History on Enthalpy Relaxation in Glassy Polymers. 3. Experimental and Modeling Studies of Polystyrene

Ian M. Hodge* and Gary S. Huvard

The BFGoodrich Company, Research and Development Center, Brecksville, Ohio 44141.
Received May 5, 1982

ABSTRACT: The relaxation component of the heat capacity at constant heating rate (10 K min^{-1}) of a polydisperse polystyrene as a function of previous cooling rate, annealing time, and annealing temperature is accurately predicted by an adaptation of an algorithm due to Moynihan using parameter values determined from an analysis of the glass transition kinetics of a single thermal history. For this material, the annealing behavior below T_g is determined by the same kinetic parameters that describe the glass transition phenomenon. A similar analysis of published data for a monodisperse polystyrene indicates that the monodisperse material has a broader distribution of relaxation times and is more nonlinear. The parameter optimization method used appears to be sufficiently sensitive to permit routine characterization of the enthalpy relaxation of amorphous materials.

Introduction

Annealing of polymers below the glass transition temperature range results in a decrease in enthalpy, which is recovered during reheating to above the transition range. This recovery is manifested as an endothermic peak or inflection in the heat capacity at temperatures ranging from well below[1-7] to the upper edge[8-10] of the glass transition range. A review of experimental aspects of this phenomenon has been given by Petrie.[10] Sufficient data have now been published to permit several generalizations to be made: (1) The decrease in enthalpy during annealing, ΔH, and the temperature at which the heat capacity maximum occurs, T_{max}, are both increasing linear functions of annealing temperature T_e when T_e is more than ca. 30 K below T_g. When T_e is about 20 K below T_g, ΔH passes through a maximum and then decreases with increasing T_e. (2) ΔH and T_{max} are linear functions of log t_e (t_e = annealing time) when t_e is sufficiently short that the annealed glass is still far from equilibrium. At long t_e, ΔH becomes constant as the annealed glass approaches equilibrium. (3) Both ΔH and the value of C_p at T_{max}, C_{pmax}, increase with heating rate Q_H. T_{max} increases approximately linearly with log Q_H.

Kovacs et al.[11] and Hodge and Berens[12] have demonstrated that sub-T_g peaks result from the nonexponentiality and nonlinearity of the glass transition kinetics. Hodge and Berens also demonstrated that all of the experimental observations listed above are reproduced by applying the successful treatment of glass transition kinetics described by Moynihan and co-workers[13] to thermal histories, which included annealing. In addition, a good description of T_{max} and C_{pmax} as a function of T_e and t_e for poly(vinyl chloride) (PVC) was obtained.[12]

Although the validity of applying Moynihan's formulation to annealing effects is well supported by the reproduction of the general trends listed above, its reproduction of the data for PVC is not a good quantitative test of its accuracy for several reasons. First, the amount of "crystallinity" in the PVC (as measured by the area of the broad endotherms well above T_g) was not closely controlled, and in view of suggestions that crystallinity may immobilize chain segments in the amorphous phase at the interface,[14-16] the possibility exists that the distribution of relaxation times (or nonexponentiality) differed from one sample to another. Also, it is known that the breadth of the glass transition increases with crystallinity in several polymers,[15] and since this breadth is determined by a number of factors in addition to the distribution width (e.g., activation energy and nonlinearity), it is possible that other aspects of the glass transitions were affected as well. Second, the PVC powder was quenched into liquid nitrogen in order to accelerate the annealing process, so that the cooling rate through T_g could only be estimated. Finally, the extraction of parameters from the experimental data was performed by a subjective judgment of goodness of fit.

The work described here was motivated by the need to test the application of Moynihan's formulation to annealing more rigorously. For this purpose a completely amorphous polymer, atactic polystyrene (PS), was chosen and all cooling, annealing, and reheating were performed in the DSC instrument under controlled conditions. Model parameters were obtained from experimental data for a single thermal history by the optimization procedure described below, and the model was tested by comparing predictions for other thermal histories with experimental data. Since it was not our purpose to compare the merits of the Moynihan approach with any other description (e.g., that of Kovacs et al.[11]), other formulations were not tested.

The Model

For convenience, we give a brief account of Moynihan's treatment and how annealing is introduced. A full description is given elsewhere.[12] Enthalpy relaxation is calculated from Boltzmann superposition of responses to the total thermal history by considering cooling and

0024-9297/83/2216-0371$01.50/0